Radial decomposition of blade vibration to identify stall flutter source in a transonic fan

Conference Paper · September 2018

CITATIONS
2

READS
103

3 authors:

Quentin Rendu
Atomic Energy and Alternative Energies Commission
32 PUBLICATIONS **230** CITATIONS
SEE PROFILE

Loïc Salles
University of Liège
136 PUBLICATIONS **2,618** CITATIONS
SEE PROFILE

Mehdi Vahdati
Imperial College London
172 PUBLICATIONS **4,308** CITATIONS
SEE PROFILE

RADIAL DECOMPOSITION OF BLADE VIBRATION TO IDENTIFY STALL FLUTTER SOURCE IN A TRANSONIC FAN

Q. Rendu*
Rolls-Roys VUTC,
Mechanical Engineering Department,
Imperial College London,

L. Salles
Rolls-Roys VUTC,
Mechanical Engineering Department,
Imperial College London

M. Vahdati
Rolls-Roys VUTC,
Mechanical Engineering Department,
Imperial College London

ABSTRACT

This paper investigates the three-dimensionality of the unsteady flow responsible for stall flutter instability. Nonlinear unsteady RANS computations are used to predict the aeroelastic behavior of a fan blade at part speed. Flutter is experienced by the blades at low mass flow for the first flap mode at nodal diameter 2. The maximal energy exchange is located near the tip of the blade, at 90% span. The modeshape is radially decomposed to investigate the main source of instability. This decomposition method is validated for the first time in 3D using a time-marching nonlinear solver. The source of stall flutter is finally found at 65% span where the local vibration induces an unstable oscillation of the shock-wave of large amplitude. This demonstrates that the radial propagation of the unsteady flow must be taken into account to predict stall flutter.

INTRODUCTION

Aeroelasticity is one of the main concerns during the design of future jet engines. Due to large diameter and light materials, flutter may be experienced by fan blades. Computational Fluid Dynamics (CFD) is used to predict fan flutter boundary in the early design steps. In the recent years, efforts have been done to build 3D model of fan flutter. These models are accurate enough to describe the flutter boundary of an engine fan, eventually taking into account acoustic wave reflections at the intake [1]. These computations show that the exchange of energy between the fluid and the structure is mainly done between 80% and 90% of the blade height [2, 3]. Thus, the damping coefficient of the blade is sometimes approximated by 2D computations near the blade tip.

During stall flutter, the blades vibration generate shock-wave oscillations, fluctuations of the boundary layer and propagation of acoustic waves in the three directions. The interactions of all these unsteady mechanisms leads to aerodynamic forces whose resultant is destabilising. Because of these interactions, the identification of flutter sources is a real challenge. Detailed analysis of the unsteady flow provides insights but may not be sufficient. To overcome this challenge, one can decompose the response of the flow into a sum of responses to elementary perturbations. Such a decomposition relies on the linearity of the flow with respect to time. This approach has been used by Ferrand [4] to analyse choke flutter contributions using a coupled 1D/2D linearised Euler method. It has recently been extended to two dimensional turbulent flow using a linearised RANS solver [5]. The present work aims at extending the method to three dimensional flows using a nonlinear time-marching RANS solver.

The test case and the numerical methods are presented in the next section. The decomposition method is then validated on stall flutter using a 3D nonlinear RANS solver. The method is finally used to identify the radial layer driving the aeroelastic instability.

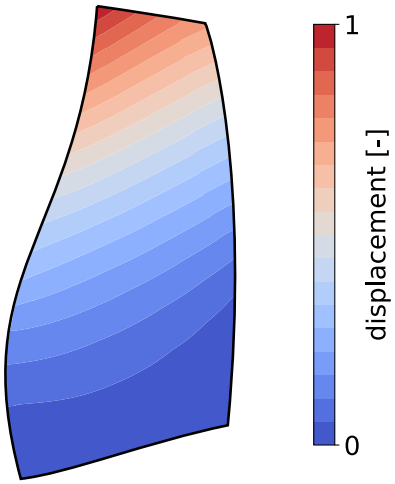

FIGURE 1. Normalised displacement for the first flap mode (1F)

1 Methods

1.1 Test case

The study is performed on a low-speed fan consisting of 20 wide-chord blades. The Mach number of the blade tip is used to characterise the rotational speed:

$$M_{tip} = \omega r_{tip}/a \tag{1}$$

A flutter zone has been measured experimentally at part speed ($0.86 < M_{tip} < 0.98$). The involved modeshape corresponds to the first flap mode (1F) at nodal diameter 3ND. The normalised displacement associated with this modeshape is shown in Fig. 1. The corresponding reduced frequency, based on relative velocity and chord at 90% span, is 0.12.

1.2 Computational methods

The Unsteady Reynolds-Averaged Navier-Stokes (URANS) solver AU3D is used to perform all the computations. It has been developped at Imperial College with the support of Rolls-Roycs and has been extensively validated over the past 25 years. It relies on a time-domain finite volume method on multi-block unstructured grid. The turbulence is modelled through Spalart-Allmaras model with wall functions [6]. More details can be found in [7].

The computational domain consists of a single-passage fan blade without tip clearance. Total pressure, total temperature and flow angles are prescribed at the domain inlet. Static pressure is prescribed at the domain outlet. For steady computations, periodic boundary conditions are used on the sides of the domain. For aeroelastic simulations, a phase-lagged boundary condition is used to compute the different nodal diameters [8]. The vibration of the blade is imposed during the simulation and the resulting aerodynamic forces are used to compute the work. To avoid acoustic reflections, annular ducts extend the mesh upstream and downstream of the fan. The axial length of mesh cells is increased to damp the pressure waves. The hub and casing surfaces are treated as inviscid to allow inviscid inlet boundary condition. The resulting computational domain is presented in Fig. 2. It contains 20 layers in the spanwise direction and around 250 points on the blade profile, resulting in 130,000 total points, which allows very low turnaround time.

FIGURE 2. Computational mesh for aeroelastic computations (fan blade in orange)

2 Results and Discussion

2.1 Flutter onset

The rotational speed is chosen in the middle of the experimental flutter zone ($M_{tip} = 0.91$). Aeroelastic computations are run at different massflows along this speedline to identify the flutter zone. The damping coefficient obtained for nodal diameters 2ND and 3ND are plotted in Fig. 3. Close to the design point ($m/m_{ref} > 0.95$), the damping coefficient is positive for both nodal diameters, indicating aeroelastic stability. The aerodyanmic damping decreases when the massflow decreases, until reaching the flutter zone at $m/m_{ref} = 0.78$ for nodal diameter 3ND and at $m/m_{ref} = 0.82$ for nodal diameter ND=2. The most unstable nodal diameter is 2ND whereas flutter was measured for ND=3 experimentally. This discrepancy comes from the air intake which is not included here while it largely contributes to stall flutter through reflection of acoustic waves [9].

The steady streamlines and axial velocity are plotted in Fig. 4 for two different massflows. The flow is coming from the left, forming a supersonic region behind the leading edge, terminated by a strong shock-wave. Outside of the flutter zone ($m/m_{ref} = 0.86$), the streamlines are mainly axial and the flow is attached to the blade. At $m/m_{ref} = 0.79$, a radial migration of the flow appears, leading to a low axial velocity zone from 50% chord to the trailing edge. This radial pattern is typical of stall flutter events [3].

All the following computations are obtained for the flutter case, *i.e.* $m/m_{ref} = 0.79$ and ND=2. In the next section, the radial decomposition of the modeshape is evaluated.

2.2 Validation of radial decomposition method

To compute the contribution of each radial layer to the global damping coefficient, the modeshape is decomposed into ten panels as shown in Fig. 5. All the panels have the same number of points and include two radial levels of the mesh. Ten unsteady computations are run, each of them with one panel vibrating. The

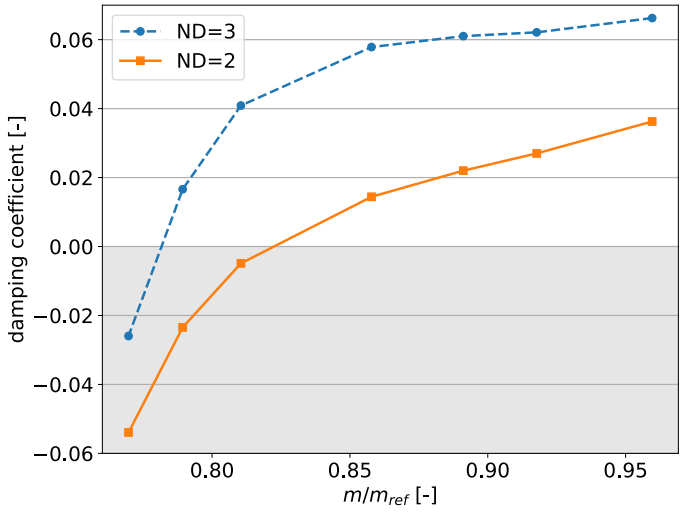

FIGURE 3. Damping coefficient along massflow for nodal diameters ND=2 and ND=3

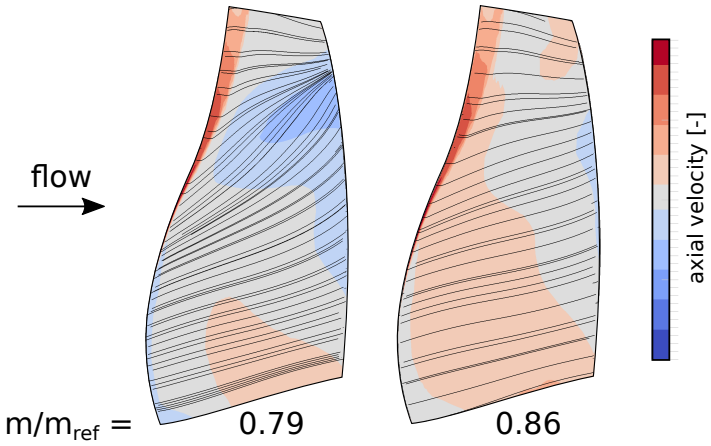

FIGURE 4. Streamlines and axial velocity on suction surface at $m/m_{ref} = 0.79$ and $m/m_{ref} = 0.86$

3D unsteady pressure is then projected on the full modeshape to compute the work extracted by the flow.

The decomposition of the unsteady flow in the sum of unsteady flows relies on the linear superposition principle. To stay in the linear regime, a small vibration amplitude is imposed and the computations are run until a periodic state is reached. The results presented here are obtained after 50 vibration cycles.

The damping coefficient obtained with radial decomposition method is compared with a full blade vibration in Fig. 6. Both methods yield the same results. The global damping coefficient predicted with full modeshape and sum of panels are 2.378×10^{-2} and 2.390×10^{-2} respectively (0.5% error).

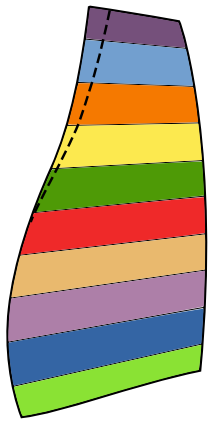

FIGURE 5. Radial decomposition of the modeshape in ten panels - dashed line denotes the steady position of the shock-wave

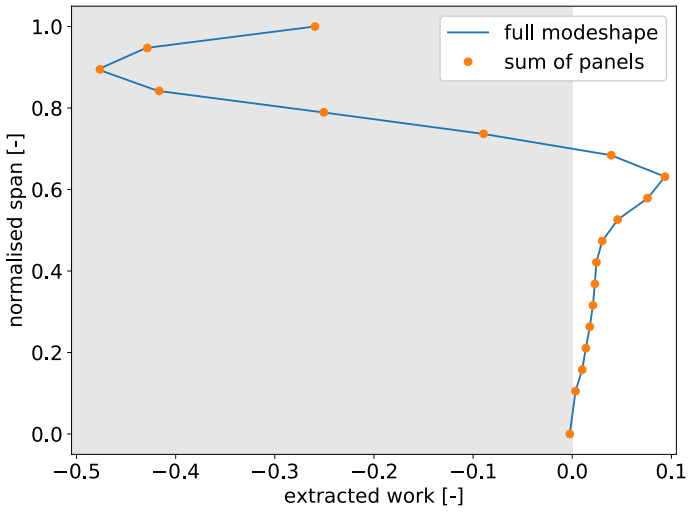

FIGURE 6. Work extracted by the flow along span for the full blade vibration (solid line) and the decomposition method (symbols)

At each radial level, the damping coefficient is the integral of the work extracted by the flow. Some local discrepancies may thus compensate and disappear when looking only at the global coefficient. To further validate the radial decomposition method, the local work extracted by the flow at tip is plotted in Fig. 7. The peak of stabilising work at 25% chord corresponds to the unsteady oscillation of the strong shock-wave on the suction surface. This stabilising contribution is counteracted by the destabilising contributions of the suction surface downstream of the shock-wave as well as on the pressure surface. Once again, both methods yield the same results.

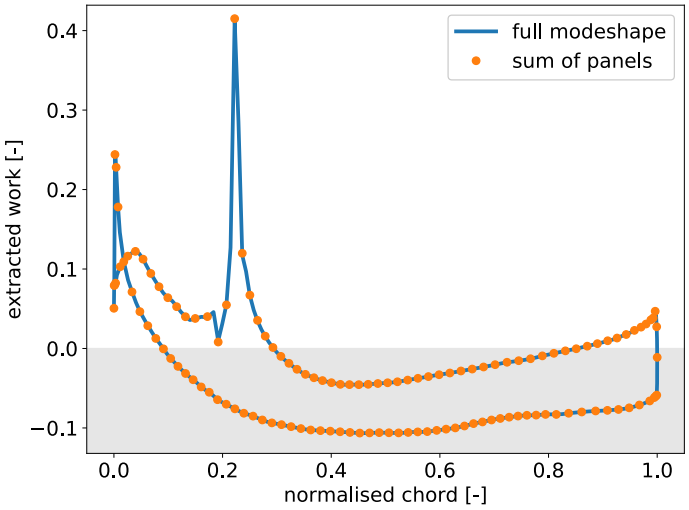

FIGURE 7. Work extracted by the flow along chord at tip section for the full blade vibration (solid line) and the decomposition method (symbols)

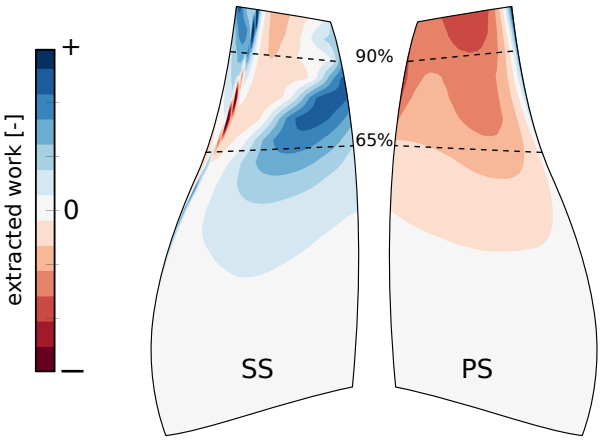

FIGURE 8. Normalised work extracted by the flow on blade suction surface (SS) and pressure surface (PS) for the full blade vibration - negative (red) depicts instability

2.3 Local analysis of the work

Flutter is a self-induced aeroelastic instability. Vibration of the blades generate unsteady flow (pressure and velocity fluctuations). These fluctuations then propagate until reaching a part of the blades where energy is exchanged between the fluid and the structure. Flutter can thus be described as an emission/reception mechanism where the blade is both emitter and receiver of pressure fluctuations (unsteady loads).

The extracted work plotted along span in Fig. 6 gives insights on the reception part, *i.e.* where the exchange of energy occurs. One can see that the minimal damping coefficient is found at 90% span. This is typical for fan flutter because of the large displacements near the tip. The oscillation of the shock-wave, which strength increases with radius, may also generate large pressure fluctuations [2]. To perform a more detailed analysis, the work extracted by the flow on the blade surface is plotted in Fig. 8.

Two large regions are associated with destabilising work. The largest corresponds to the pressure surface from around 10% of the chord until the trailing edge. In this region, the amplitude of negative work increases with radius, giving the most destabilising contribution at tip. Another large destabilising region is located on the suction surface. It starts with a destabilising shock-wave oscillation between 70% and 80% span and then migrates radially. From 90% to the blade tip, around 50% of the chord is associated with a destabilising work, which amplitude slightly increases with radius.

Two regions are associated with stabilising work. The largest one starts at 50% span on suction surface and develop towards the trailing edge at 90% span. This region corresponds to the low axial velocity zone (see Fig. 4). Once again the amplitude of extracted work increases with radius. The other stabilising region starts at 85% span close to the leading edge and develops radially. From 90% span, it includes the shock-wave whose contribution switches from destabilising to stabilising.

To summarise, the pressure surface is always destabilising, with a contribution increasing with the radius (maximal at tip). On the suction surface, there's at each radial level a competition between stabilising and destabilising regions. Below 90% span, the destabilising shock-wave is counteracted by the stabilising low axial velocity zone. Above 90% span, the destabilising mid-chord region is counteracted by the stabilising shock-wave. As a result, the least stable radial level does not include any of the largest destabilising regions but lies on the frontier between them.

2.4 Identification of stall flutter source

The regions of main energy exchange have been identified in the previous section. This answered the question: *Where do the pressure fluctuations reach the blade ?* (reception mechanism). The question corresponding to the emission mechanism would be: *Where do the pressure fluctuations come from ?* This last section aims at answering this question using the radial decomposition method.

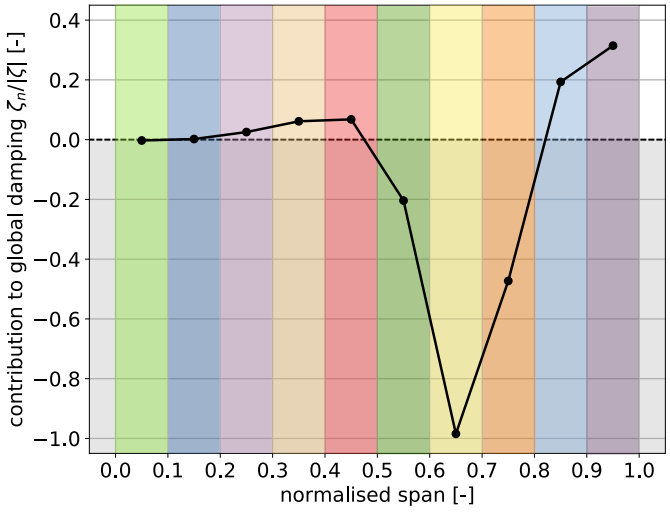

FIGURE 9. Contribution of each panel to the global damping (see Fig. 5 for corresponding colors)

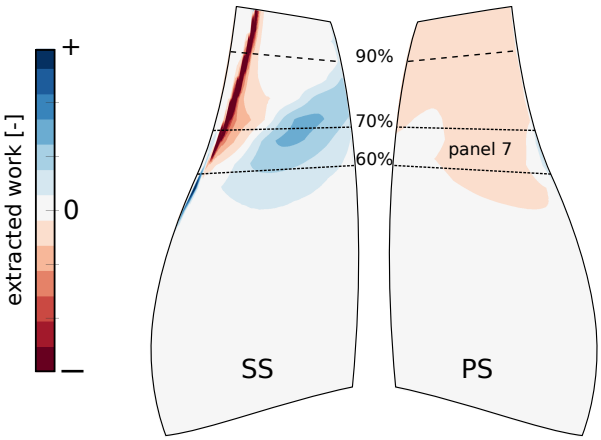

FIGURE 10. Normalised work extracted by the flow on blade suction surface (SS) and pressure surface (PS) for the vibration of panel 7 - negative (red) depicts instability

By applying the radial decomposition method to the ten panels shown in Fig. 5, ten 3D unsteady fields are obtained. The damping coefficient ζ_n, associated to the panel n (where $n \in [1,10]$), is obtained by projecting the unsteady pressure field $p_n(\mathbf{x},t)$ on the full modeshape. ζ_n can be referred as the contribution of panel n to the global damping. As mentioned in Sect. 2.2, the sum of the contribution ζ_n is equal to the global damping with a relative error equal to 0.5%.

The contribution of each panel to the global damping is plotted in Fig. 9. The abscissa corresponds to the spanwise position of each panel and the background colors refer to the panel position in Fig. 5. Starting the analysis from the blade root, the two first panels show a negligble contribution to the global damping. This is expected as the displacement is very small close to the root. The following panel ($h = 0.25$) exhibits a small stabilising contribution. It increases slightly with span until $h = 0.45$. This corresponds to the increase in displacement amplitude. The contribution of the lower half of the blade is given by

$$\frac{\zeta_{low}}{|\zeta|} = \sum_{n=1}^{5} \frac{\zeta_n}{|\zeta|} = 15.4\% \qquad (2)$$

The first half of the blade has a small stabilising contribution.

The contribution of the sixth panel ($h = 0.55$, dark green) is significantly destabilising. This high contribution is explained by the oscillation of the shock-wave whose steady position reaches $h = 0.5$ (see Fig. 5). It is thus excited by the local blade vibration. The next panel ($h = 0.65$, yellow) shows the maximal contribution $\zeta_7/|\zeta| = -98.5\%$. The contribution increases sharply with span until recovering stability for the two last panels ($0.8 < h < 1.0$).

This analysis shows that only three panels are responsible for destabilising contributions. The panel 7, located at $h = 0.65$ contributes almost 100% to the global damping. The effect of all the other panels globally cancel each other (while locally the work will unlikely be cancelled).

To understand why the panel 7 ($0.6 < h < 0.7$) gives the largest contribution to the aeroelastic behaviour of the blade, the local work associated to its vibration is plotted in Fig. 10. Some regions show a behaviour similar to the full blade vibration (Fig. 8). In both case the pressure side contributes negatively to the global damping. When the panel 7 vibrates, this contribution is however weaker and doest not increase with span. On the suction side, the stabilising region correlated with low steady axial velocity is still observed. It is smaller and weaker than for the full blade vibration.

The main difference comes from the shock-wave response which is now largely destabilising from 60% span to tip. A region of large negative work is also found downstream of the shock-wave around 70% span. Such a behaviour may be associated with shock-wave boundary-layer interaction [10]. Below 70% span, close to the leading edge, a stabilising effect of the shock-wave can be observed. If the contribution of the shock-wave is stabilising below the panel and destabilising above, it would explain the stability increase from $h = 0.7$ (see Fig. 9). To evaluate this hypothesis, the work extracted on the suction surface for the vibration of panels 6 to 9 is plotted in Fig. 11. The panel 6 is the first one to impact the shock-wave, whose contribution is destabilising until the tip. The panel 7 shows the aforementioned unstable shock-wave behavior above

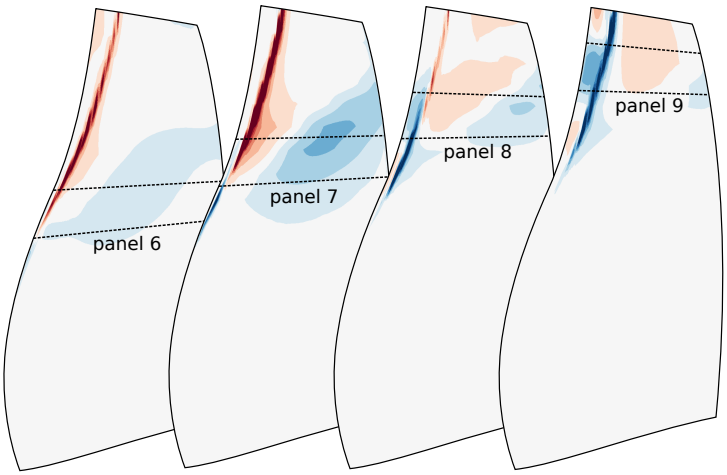

FIGURE 11. Normalised work extracted by the flow on blade suction surface for the vibration of panels 6 to 9 - negative (red) depicts instability

and stable below. Above panel 8, the shock-wave still has a destabilising contribution but of weaker amplitude. Below panel 8 a strong stabilising contribution of the shock-wave is rising. For panel 9 and 10 (not shown here), a large stabilising contribution of the shock-wave is observed. Therefore, the transition of the shock-wave contribution cannot be explained by a simple model of local excitation. In particular, one expects the trailing edge to generate acoustic waves which interact with the shock-wave to modify its contribution [11].

While the mechanisms driving the shock-wave contribution may still be unclear, this section clarified the emitter mechanism associated to flutter. It has been shown that the unstable contribution of the tip of the blade is not triggered by its local vibration. The main source of destabilising unsteady loads is found at 65% span and impacts the aeroelastic behaviour of the tip by driving an unstable oscillation of the whole shock-wave.

CONCLUSION

In this paper, the mechanisms leading to stall flutter have been investigated. Flutter was observed at part-speed and low massflow for a transonic fan blade. The involved modeshape is the first flap (1F) mode along nodal diameter 2ND at low reduced frequency. Aeroelastic simulations are able to reproduce the flutter event and the least stable radial level is found at 90% span.

To understand what drives this destabilising exchange of energy, the modeshape has been radially decomposed into ten panels which can vibrate independently. This radial decomposition method, initially proposed for linear solver, has been successfully validated using a 3D nonlinear RANS solver.

This method shows that the local vibration of the blade above 80% is stabilising. The source of the flutter is located around 65% span, far below the least stable radial level. The vibration at this span leads to an oscillation of the whole shock-wave, generating large destabilising unsteady loads from 65% span to the tip. This demonstrates that the radial propagation of the unsteady loads must be taken into account to predict stall flutter.

The transition of the shock-wave contribution from destabilising around mid-span to stabilising close to the tip, has not been explained. The radial decomposition presented here indicates that the span plays an important role, but does not allow to distinguish between the local excitation of the shock-wave and the impact of pressure waves generated at the trailing edge. To address this challenge, the panels can be further decomposed into smaller patches covering the shock-wave root and the trailing edge.

Another perspective is to include the effects of acoustic reflections at air intake and the influence of the tip leakage on the stability. At this stage, using a linearised RANS solver would prevent too large computational costs.

ACKNOWLEDGMENT

The authors would like to thank Rolls-Royce plc for funding this work and allowing its publication.

REFERENCES

[1] Zhao, F., Smith, N., and Vahdati, M., 2017. "A simple model for identifying the flutter bite of fan blades". *Journal of Turbomachinery,* ***139***(7), p. 071003.

[2] Aotsuka, M., and Murooka, T., 2014. "Numerical analysis of fan transonic stall flutter". In ASME Turbo Expo 2014: Turbine Technical Conference and Exposition, American Society of Mechanical Engineers, pp. V07BT35A020–V07BT35A020.

[3] Vahdati, M., and Cumpsty, N., 2016. "Aeroelastic instability in transonic fans". *Journal of Engineering for Gas Turbines and Power,* ***138***, Feb.

[4] Ferrand, P., 1984. "Linearized theory of the choked flow in an annular oscillating cascade". In Unsteady Aerodynamics and Aeroelasticity of Turbomachines and Propellers, 3rd International Symposium, Ed Cambridge University, pp. 41–52.

[5] Rendu, Q., Aubert, S., and Ferrand, P., 2017. "Influence of reduced frequency on choke flutter in transonic UHBR fan". In International Forum on Aeroelasticity and Structural Dynamics.

[6] Spalart, P., and Allmaras, S., 1992. "A one-equation turbulence model for aerodynamic flows". In 30th Aerospace Sciences Meeting.

[7] Sayma, A., Vahdati, M., and Imregun, M., 2000. "An integrated nonlinear approach for turbomachinery forced response prediction. part i: Formulation". *Journal of fluids and structures,* ***14***(1), pp. 87–101.

[8] Stapelfeldt, S., and di Mare, L., 2013. "Modelling rotor-rotor interaction on reduced passage counts". In 10th European Conference on Turbomachinery.

[9] Vahdati, M., Simpson, G., and Imregun, M., 2011. "Mechanisms for wide-chord fan blade flutter". *ASME J. Turbomachinery,* ***133***(4).

[10] Rendu, Q., Rozenberg, Y., Aubert, S., and Ferrand, P., 2017. "Influence of acoustic blockage on flutter instability in a transonic nozzle". *ASME J. Turbomachinery*.

[11] Atassi, H., Fang, J., and Ferrand, P., 1995. "Acoustic blockage effects in unsteady transonic nozzle and cascade flows". In 33rd AIAA Aerospace Sciences Meeting.